Physics Letters A 376 (2012) 610–615

Contents lists available at SciVerse ScienceDirect

Physics Letters A

www.elsevier.com/locate/pla

Edge states at the interface between monolayer and bilayer graphene

Zi-xiang Hu [a,b,*], Wenxin Ding [c]

[a] Department of Physics, ChongQing University, ChongQing, 400044, China
[b] Department of Electrical Engineering, Princeton University, Princeton, NJ 08544, USA
[c] NHMFL and Department of Physics, Florida State University, Tallahassee, FL 32306, USA

ARTICLE INFO

Article history:
Received 31 August 2011
Received in revised form 22 November 2011
Accepted 22 November 2011
Available online 3 December 2011
Communicated by R. Wu

Keywords:
Edge state
Hybrid
Dirac equation

ABSTRACT

The electronic properties for monolayer–bilayer hybrid graphene with zigzag interface are studied by both the Dirac equation and numerical calculation in zero field and in a magnetic field. Basically there are two types of zigzag interface dependent on the way of lattice stacking at the edge. Our study shows they have different locations of the localized edge states. Accordingly, the energy-momentum dispersion and local density of states behave quit differently along the interface near the Fermi energy $E_F = 0$.

1. Introduction

In recent years, the experimental accessibility of the single and multilayered graphene samples [1–5] has attracted considerable theoretical and experimental attentions due to its unusual electronic structure described by the Dirac equation, namely electrons in monolayer graphene have linear dispersion thus behave like massless Dirac fermions at the corners of the Brillouin zone (BZ) [6]. In the presence of magnetic field perpendicular to the graphene plane, the system shows anomalous integer quantum Hall effect [7–10] (IQHE) which is also different from that of the conventional two-dimensional electron system in semiconductor heterostructures. The Hall conductivity in the IQHE of graphene shows plateaus at $\sigma_{xy} = 4(N + 1/2)e^2/h$, in which the factor 4 comes from the four-fold valley and spin degeneracy and the shift $1/2$ reflects particle–hole symmetry in the 0'th Landau level.

Edge states in graphene have been the focus of much theoretical study because of the important role they play in the transport [11]. It is well known that there are two basic types of edges in graphene, namely, the armchair and zigzag edges. Some theoretical works [12–26] on the electronic structure of finite-sized systems, either as molecules or as one-dimensional systems, have shown that zigzag edged graphene has localized state near the Fermi energy, but those with armchair edge do not have such state. Therefore, the transport properties are very different due to the existence of the edge state. On the other hand the hybrid edge structure, composed of partial monolayer and partial bilayer graphene, which is quit general in reality, hasn't received so much attention. Experimentally [28] the anomalous quantum oscillations in magnetoconductance were observed due to the peculiar physics along the interface. After the experimental study, we presented our studies of the electronic properties of the hybrid interface of graphene in the APS meeting [29]. Recently we noticed there are some new experiments and correlated theoretical studies [32,33] on this topic. Thus we decided to present our systematical study of the edge states of the hybrid interface.

In this work, we study the electronic properties of the hybrid interface via both tight-binding model and its effective theory in the continuum limit – the Dirac equation. The edge states in graphene can be studied experimentally by using a local probe such as scanning tunneling microscopy (STM). The STM experiments measure the differential conductance which is proportional to the density of states. Numerically we can study the local density of states (LDOS) which is defined as [27]:

$$N(r, eV) = \left|\Psi_\alpha(r)\right|^2 \delta(eV - E_\alpha), \tag{1}$$

where $\Psi_\alpha(r)$ is the eigenfunction with energy E_α. The LDOS shows the strength of the local electronic density which is related to the strength of the signal in STM experimental data. Our study of the hybrid edge graphene shows that there are always zero energy states localized near the zigzag hybrid edge although the distribution of LDOS of these edge states strongly depends on the details of how the edge stacks together. The dispersion curve around the Dirac cones also shows different characters for different edge arrangements either within or without a magnetic field.

* Corresponding author at: Department of Electrical Engineering, Princeton University, Princeton, NJ 08544, USA.
E-mail address: zihu@princeton.edu (Z.-X. Hu).

0375-9601/$ – see front matter
doi:10.1016/j.physleta.2011.11.046

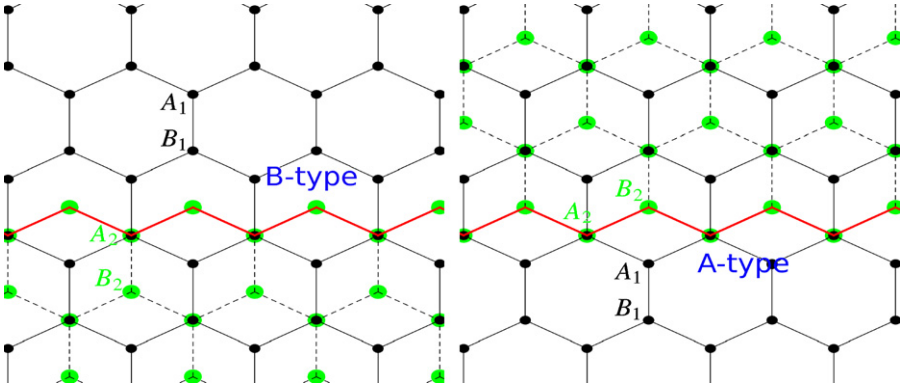

Fig. 1. (Color online.) The schematic pictures for two kinds of hybrid monolayer–bilayer interfaces. The atoms of the extended bottom layer (layer 1) are indicated by black dots (smaller) while the green dots (larger) represent the top layer (layer 2) which terminates at the interface. In the left plot, the top layer is ended with B_2 sites (B-type) while on the right it is ended with A_2 sites (A-type).

This Letter is arranged as follows: In Section 2, we set up the model Hamiltonian in different geometries. The zero energy solutions in zero field and in magnetic field are obtained by solving the Dirac equations. The numerical results in a finite system are shown in Sections 3 and 4. Some discussions and conclusions are in Section 5.

2. Model and different geometries

We consider a bilayer graphene with Bernal stacking, as shown in Fig. 1; its tight-binding Hamiltonian can be written as:

$$H = -t\sum_{i=1}^{2}\sum_{m,n} a^{\dagger}_{i;m,n}(b_{i;m,n} + b_{i;m-1,n} + b_{i;m,n-1}) - t_{\perp}\sum_{m,n} a^{\dagger}_{2;m,n} b_{1;m,n} + \text{h.c.}, \tag{2}$$

where $a_{i;m,n}$ ($b_{i;m,n}$) is the annihilation operator at position $(m,\ n)$ in sublattice A_i (B_i), and $i = 1, 2$, indicating the two different layers. The first term is the Hamiltonian within each layer, and the second term describes the interlayer coupling in which we only consider the hopping between the two atoms stacked right on top of each other. Let us label the bottom (extended) layer as layer 1, the half-plane upper layer as layer 2. In this work we will only consider the Bernal stacking. One can expand the effective Hamiltonian near the two Dirac points K and K' which are time reversal symmetric partners. In momentum space, the Hamiltonian near K can be written as:

$$H = \sum_{k} \Psi^{\dagger}_{k} \cdot H_k \cdot \Psi_k, \tag{3}$$

where

$$H_k = \begin{pmatrix} 0 & v_F k & 0 & 0 \\ v_F k^* & 0 & t_{\perp} & 0 \\ 0 & t_{\perp} & 0 & v_F k \\ 0 & 0 & v_F k^* & 0 \end{pmatrix} = v_F \begin{pmatrix} 0 & k & 0 & 0 \\ k^* & 0 & \gamma & 0 \\ 0 & \gamma & 0 & k \\ 0 & 0 & k^* & 0 \end{pmatrix}, \tag{4}$$

in which $k = k_x + ik_y$, $\gamma = t_{\perp}/v_F$, and $\Psi_k = (a_{1;k}, b_{1;k}, a_{2;k}, b_{2;k})$. For the other Dirac point, as stated before, $H_{K'} = H^*_K$. Here we only consider the zigzag type interface (or edge) to explore the localized edge state. Without magnetic field and the interface, it is sufficient to discuss just one Dirac cone in the continuum model due to the symmetry. But with the interface breaking the inversion symmetry and the magnetic field breaking the time reversal symmetry, the two Dirac points are not equal to each other, and both must be studied.

According to the lattice orientation we adopt as shown in Fig. 1, the zigzag interface is along the x direction. For simplicity, we consider an infinite stripe along the x direction, therefore the system has translational symmetry along the x direction thus k_x remains a good quantum number. We then do Fourier transformation in the x direction and reduce the 2D problem to 1D. There are actually TWO distinct geometries which are physically different. i) The outmost sites of the upper layer are the B_2 sites which do not stack directly on the lower layer atoms as shown in Fig. 1 (left). The B_2 sites are the low energy degrees of freedom (along with A_1) which are kept if one further considers a 2×2 effective theory on energy scale $\epsilon \ll t_{\perp}$. We label it the B-type stacking according to the type of the outmost atoms; ii) A-type stacking, i.e., the A_2 sites are the outmost sites on the upper layer as shown in Fig. 1 (right). The A_2 sites, together with the B_1 sites which they stack right on top of, form the dimer sites. In the 2×2 low energy effective theory the wavefunctions have almost zero weight on those dimes sites when $\epsilon \ll t_{\perp}$. As a result these dimers are ignored in this limit. In the other words, they are occupied considerably only at high energy (comparing to $t_{\perp}$).

3. Interface properties in zero field

For a semi-infinite sheet, it is well known that the existence of the zero energy edge modes in both monolayer and bilayer graphene. Presumably, such modes are also expected at the interface between them. Let us consider the following geometry: a half-plane of monolayer graphene and a half-plane of bilayer graphene joined along the zigzag edge; and look for solution(s) with zero eigen-energy by using the Dirac equation.

$$\Psi_{\text{mono}}(x, y) = \begin{pmatrix} \psi_A(x, y) \\ \psi_B(x, y) \end{pmatrix} \tag{5}$$

and

$$\Psi_{\text{bi}}(x, y) = \begin{pmatrix} \psi_{A1}(x, y) \\ \psi_{B1}(x, y) \\ \psi_{A2}(x, y) \\ \psi_{B2}(x, y) \end{pmatrix} \tag{6}$$

are the wavefunctions at Dirac point in the monolayer and bilayer respectively. Assuming the interface locates at $y = 0$, the boundary condition for monolayer is then straightforward: both components of the wavefunction must be continuous. For the upper layer, it terminates at $y = 0$ and therefore satisfies the open boundary condition. Note that the term 'terminates' indicates the last row of lattice sites are the high/low energy sites (A_2/B_2), however, the boundary condition is not the wavefunctions being zero on these sites. They should be the wavefunctions of the sites one

unit cell 'outside' the boundary being zero. Therefore, at the edge, the wavefunctions satisfy [31]:

$$\psi_A(x,0)=\psi_{A1}(x,0),\qquad \psi_B(x,0)=\psi_{B1}(x,0),$$
$$\begin{cases}\psi_{A2}(x,0)=0 & \text{B-type},\\ \psi_{B2}(x,0)=0 & \text{A-type}.\end{cases} \tag{7}$$

In the monolayer region with zigzag interface, we do the substitution $k\to k_x+\partial_y$ in the Dirac Hamiltonian $H_{\text{mono}}=v_F\left(\begin{smallmatrix}0 & k\\ k^* & 0\end{smallmatrix}\right)$ [11]. The zero energy solution is

$$\begin{cases}\phi_A(y)=e^{yk_x}C_2,\\ \phi_B(y)=e^{-yk_x}C_1.\end{cases} \tag{8}$$

In analogy, we do the same substitution in the bilayer Hamiltonian (Eq. (4)) and obtain its zero energy solution:

$$\begin{cases}\phi_{B1}(y)=e^{-yk_x}A_1,\\ \phi_{B2}(y)=-e^{-yk_x}y\gamma A_1+e^{-yk_x}A_2,\\ \phi_{A1}(y)=e^{yk_x}A_3+e^{yk_x}y\gamma A_4,\\ \phi_{A2}(y)=e^{yk_x}A_4.\end{cases} \tag{9}$$

Applying the boundary condition, for the B-type interface (so $\phi_{A2}(y=0)=0$), one easily finds that nonzero solutions only exist for $k_x>0$. The solution is

$$C_1=C_2=A_1=A_3=A_4=0,\qquad A_2=\text{const}. \tag{10}$$

For the A-type interface, one finds that for $k_x>0$

$$C_1=C_2=A_1=A_2=A_3=0,\qquad A_4=\text{const}. \tag{11}$$

Near the other Dirac cone, the solutions remain the same but only exist for $k_x<0$. The only nonzero constant is said to be determined by normalization. Both results are in agreement with the tight-binding analysis [30].

Even though the zero energy states exist for both types of interface, there is an important difference between them. In the case of B-type edge, the wavefunction is only nonzero in the upper layer, which is trivial as such mode is expected when a graphene sheet is terminated at a zigzag edge. However, the A-type is less trivial. The wavefunction also lives on the extended layer at the interface where no cut is present. We interpret this as following: when the dimer sites are the boundary, the interlayer coupling $t_\perp$ imposes an energy cost for electrons going through the interface in the extended layer which can be considered as an effective potential barrier. The potential barrier can localize the electron states along the interface.

We numerically diagonalize a system with a finite width up to 600 unit cells in the y direction. The intralayer hopping strength t is set to identity and the interlayer hopping strength $t_\perp=0.2t$. The dispersion relation is shown in Fig. 2. Compare the dispersions in different geometries, the A-type edge has an obviously stronger level anticrossing feature than the other. The reason is that for B-type edge, the zero energy edge state just locates on the bilayer

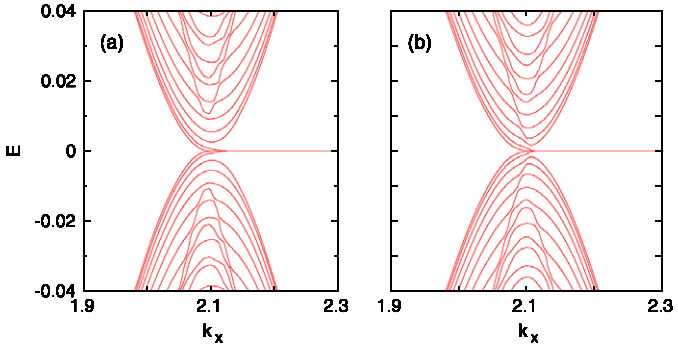

Fig. 2. The energy-momentum dispersion relation around one Dirac cone for the hybrid edge graphene with (a) B-type and (b) A-type respectively. The latter one has more energy level anticrossing near the Fermi level due to the effective potential at the edge.

graphene which has quadratic dispersion and has nothing to do with the monolayer part with a linear dispersion. However, in the case of A-type edge, the zero energy edge state also has component on the monolayer graphene at the interface, the linear dispersion part for monolayer should also connect to the edge state which induces more energy level anticrossing around the Dirac points. Fig. 3 shows the LDOS for the two kinds of hybrid graphene. We label the coordinate of the extended layer by $d\in[0,600)$ and the $d\in[900,1200)$ for upper layer. Therefore, the interface locates at $d=300$ and $d=900$ for layer 1 and 2 respectively. One can notice that the localized edge state shows as a peak at zero energy along the interface. The prominent difference is that the peak just appears on the top layer of bilayer part in the B-type case; but for the A-type case, the zero energy peak appears on both two layers although still locates at the bilayer side. The numerical results are in agreement with the analysis by the Dirac equations and we conclude that the two kinds of edge arrangements should have different consequences in experiments since the different distributions of the zero mode. Here we notice that the other peaks in LDOS at the end of the finite system is the signal of the general monolayer or bilayer zigzag edge graphene as discussed in many others work [12–26].

4. Interface properties in magnetic fields

In the presence of magnetic field, the Dirac equation should be modified by doing the substitution $\mathbf{k}\to\mathbf{k}+\frac{e\mathbf{A}}{c}$. Assume the magnetic field is along the direction of perpendicular to the plane $B=B\hat{z}$, $B>0$. We adopt the Landau gauge $\vec{A}=(A_x,A_y)=(-yB,0)$ due to the translational invariant along x direction. Thus the zero energy solution of a monolayer graphene is

$$\begin{cases}\phi_A(y)=C_1e^{k_xy-\frac{eB}{2c}y^2},\\ \phi_B(y)=C_2e^{-k_xy+\frac{eB}{2c}y^2}.\end{cases} \tag{12}$$

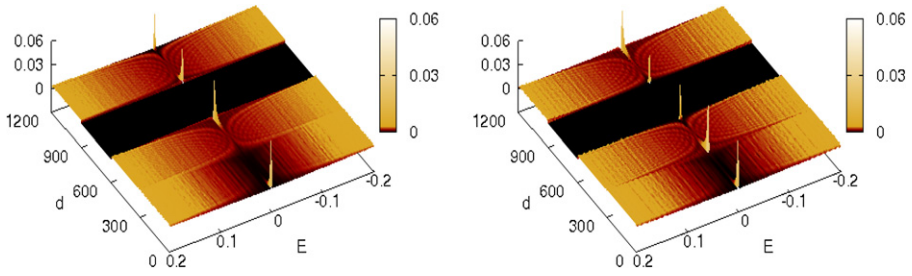

Fig. 3. (Color online.) The LDOS of the hybrid bilayer graphene with B-type (left) and A-type (right) hybrid interface respectively. The width of monolayer is 600 unit cells of honeycomb lattice. The region $d\in[0,600)$ is the lower extended layer and region $d\in[600,1200)$ is the upper layer which is cut in the middle.

Similarly, the zero energy solution for bilayer graphene becomes:

$$\begin{cases} \phi_{A1}(y) = (A_3\gamma y + A_2)e^{k_x y - \frac{eB}{2c}y^2}, \\ \phi_{B1}(y) = A_1 e^{-k_x y + \frac{eB}{2c}y^2}, \\ \phi_{A2}(y) = A_3 e^{k_x y - \frac{eB}{2c}y^2}, \\ \phi_{B2}(y) = (-A_1\gamma y + A_4)e^{-k_x y + \frac{eB}{2c}y^2}. \end{cases} \tag{13}$$

Applying the same boundary conditions as in the zero field case, we will have the solutions. For B-type, one gets

$$C_2 = A_1 = A_3 = A_4 = 0, \qquad C_1 = A_2 = \text{const.} \tag{14}$$

For A-type the solution is

$$C_2 = A_1 = A_4 = 0, \qquad C_1 = A_2 = \text{const}_1, \qquad A_3 = \text{const}_2. \tag{15}$$

The constants are determined by normalization conditions also. One immediately notices that the wavefunction lives only on the A sublattice. We should note that on the other Dirac point, the solutions remain the same form, but resides on the B sublattice. Another important feature of the solution is that for A-type we actually have TWO independent solutions here.

4.1. Dispersion relation

The Schrödinger equation in the magnetic field for a monolayer and bilayer graphene can be written as

$$\frac{1}{\sqrt{2}}\begin{pmatrix} 0 & \partial_\xi + \xi \\ -\partial_\xi + \xi & 0 \end{pmatrix}\Psi_{\text{mono}} = \epsilon\Psi_{\text{mono}} \tag{16}$$

and

$$\frac{1}{\sqrt{2}}\begin{pmatrix} 0 & \partial_\xi + \xi & 0 & 0 \\ -\partial_\xi + \xi & 0 & \tilde{\gamma} & 0 \\ 0 & \tilde{\gamma} & 0 & \partial_\xi + \xi \\ 0 & 0 & -\partial_\xi + \xi & 0 \end{pmatrix}\Psi_{\text{bi}} = \epsilon\Psi_{\text{bi}}, \tag{17}$$

where $\xi = \frac{y}{l_B} - l_B k_x$, $l_B = \sqrt{\frac{c}{eB}}$, $\epsilon = \frac{E}{\omega_c}$, $\omega_c = \sqrt{2}\frac{v_F}{l_B}$, $\tilde{\gamma} = \frac{\gamma}{v_F\omega_c}$. The solution in the bulk of the monolayer is

$$\Psi_{\text{mono}} = \begin{pmatrix} \frac{1}{\Gamma(\epsilon^2)}D_{\epsilon^2-1}(\sqrt{2}\xi) \\ \pm\frac{1}{\Gamma(\epsilon^2+1)}D_{\epsilon^2}(\sqrt{2}\xi) \end{pmatrix} = \begin{pmatrix} \psi_{\epsilon^2-1}(\xi) \\ \pm\psi_{\epsilon^2}(\xi) \end{pmatrix}, \tag{18}$$

where the $\epsilon = \pm\sqrt{N}$, $N = 0, 1, 2, \ldots$, and D_ν's are the parabolic cylinder functions, which combined with the factor $1/\Gamma(\nu+1)$ give us the eigen-wavefunctions of a harmonic oscillator $\psi_\nu(\xi)$. The bulk solution to the bilayer Hamiltonian can be written in a similar way:

$$\Phi_{\text{bi}} = \begin{pmatrix} \frac{\epsilon(\epsilon^2-(j+1)-\tilde{\gamma}^2)}{\tilde{\gamma}\sqrt{j(j+1)}}\psi_{j-1} \\ \frac{\epsilon^2-(j+1)}{\tilde{\gamma}\sqrt{j+1}}\psi_j \\ \frac{\epsilon}{\sqrt{j+1}}\psi_j \\ \psi_{j+1} \end{pmatrix}, \tag{19}$$

where $\epsilon = \pm\sqrt{\frac{1+\tilde{\gamma}^2+2j\pm\sqrt{(1+\tilde{\gamma}^2)^2+4\tilde{\gamma}^2 j}}{2}}$ $(j = 0, 1, 2, \ldots)$ is the eigen-energy.

However, for the interface problem, we need solutions on the half-plane. In this case, we put the bilayer part on the $y > 0$ side, and the monolayer part on the $y < 0$ side. Therefore, for the bilayers, the solutions on $(0, \infty)$ take on the same form as in the bulk, but j's are no longer required to be integers. Instead, we now should replace j's by

$$j_{1,2} = \epsilon^2 - \frac{1}{2} \pm \sqrt{\epsilon^2\tilde{\gamma}^2 + \frac{1}{4}}, \tag{20}$$

and ϵ now varies continuously. For the monolayer, the solution on $(-\infty, 0)$ can be chosen as

$$\Psi_{\text{mono}} = \begin{pmatrix} \psi_{\epsilon^2-1}(-\xi) \\ \mp\psi_{\epsilon^2}(-\xi) \end{pmatrix}. \tag{21}$$

With the above solutions, and combined with the boundary conditions that are already discussed in the zero field cases, we obtain the transcendental equations that dictate the dispersion relations. For the B-type interface,

$$\begin{aligned} &\big(\epsilon^2 - (j_1+1)\big)D_{j_1-1}(-\sqrt{2}k_x)\big(D_{\epsilon^2}(\sqrt{2}k_x)D_{j_2}(-\sqrt{2}k_x) \\ &\quad + D_{\epsilon^2-1}(\sqrt{2}k_x)D_{j_2+1}(-\sqrt{2}k_x)\big) \\ &= \big(\epsilon^2 - (j_2+1)\big)D_{j_2-1}(-\sqrt{2}k_x)\big(D_{\epsilon^2}(\sqrt{2}k_x)D_{j_1}(-\sqrt{2}k_x) \\ &\quad + D_{\epsilon^2-1}(\sqrt{2}k_x)D_{j_1+1}(-\sqrt{2}k_x)\big), \end{aligned} \tag{22}$$

where we have set $l_B = 1$. For the A-type, the dispersion equation is

$$\begin{aligned} &\big(\epsilon^2 - (j_1+1) - \gamma^2\big)D_{j_1}(-\sqrt{2}k_x)\big(D_{\epsilon^2}(\sqrt{2}k_x)D_{j_2}(-\sqrt{2}k_x) \\ &\quad + D_{\epsilon^2-1}(\sqrt{2}k_x)D_{j_2+1}(-\sqrt{2}k_x)\big) \\ &= \big(\epsilon^2 - (j_2+1) - \gamma^2\big)D_{j_2}(-\sqrt{2}k_x)\big(D_{\epsilon^2}(\sqrt{2}k_x)D_{j_1}(-\sqrt{2}k_x) \\ &\quad + D_{\epsilon^2-1}(\sqrt{2}k_x)D_{j_1+1}(-\sqrt{2}k_x)\big). \end{aligned} \tag{23}$$

However, one must note that in the presence of magnetic field, the time reversal symmetry is broken, therefore, the other Dirac cone, the time reversal partner, no long behaves the same way. So the dispersion relation must be calculated separately. By the same approach, one can get, for the B-type edge,

$$\begin{aligned} &\big(\epsilon^2 - j_1\big)D_{j_1}(-\sqrt{2}k_x)\big(j_2 D_{\epsilon^2}(\sqrt{2}k_x)D_{j_2-1}(-\sqrt{2}k_x) \\ &\quad + \epsilon^2 D_{\epsilon^2-1}(\sqrt{2}k_x)D_{j_2}(-\sqrt{2}k_x)\big) \\ &= \big(\epsilon^2 - j_2\big)D_{j_2}(-\sqrt{2}k_x)\big(j_1 D_{\epsilon^2}(\sqrt{2}k_x)D_{j_1-1}(-\sqrt{2}k_x) \\ &\quad + \epsilon^2 D_{\epsilon^2-1}(\sqrt{2}k_x)D_{j_1}(-\sqrt{2}k_x)\big); \end{aligned} \tag{24}$$

for the A-type edge,

$$\begin{aligned} &(j_2+1)\big(\epsilon^2 - j_1 - \gamma^2\big)D_{j_1}(-\sqrt{2}k_x)\big(j_2 D_{\epsilon^2}(\sqrt{2}k_x)D_{j_2-1}(-\sqrt{2}k_x) \\ &\quad + \epsilon^2 D_{\epsilon^2-1}(\sqrt{2}k_x)D_{j_2}(-\sqrt{2}k_x)\big) \\ &= (j_1+1)\big(\epsilon^2 - j_2 - \gamma^2\big)D_{j_2}(-\sqrt{2}k_x) \\ &\quad \times \big(j_1 D_{\epsilon^2}(\sqrt{2}k_x)D_{j_1-1}(-\sqrt{2}k_x) \\ &\quad + \epsilon^2 D_{\epsilon^2-1}(\sqrt{2}k_x)D_{j_1}(-\sqrt{2}k_x)\big). \end{aligned} \tag{25}$$

It is easy to see from the dispersion equation that when $|k_x|$ is very large, the eigen-energy should restore to either the monolayer value or the bilayer value as the parabolic cylinder functions D_ν only converge to zero for integer ν at infinity. But what interests us is how these bulk Landau levels connect with each other when crossing the interface. To study that, we solve the above equations for ϵ and k_x near the interface $k_x = 0$ for a finite-sized system as shown in Fig. 4. It is shown that the Landau levels match in different ways at two Dirac cones. Near the Dirac cone $K(K')$, the zero energy Landau levels in the bilayer region split, one branch rises up to become the $n = 1$ Landau levels in the monolayer while the other branch remains as zero energy states. The other Landau levels continues from bilayer to monolayer accordingly, i.e. $n = 1|_{\text{bi}} \to n = 2|_{\text{mono}} \ldots$. However, near the other Dirac cone $K'(K)$, the zero energy state remains intactly, so the higher Landau levels connect in the way of $n = 1|_{\text{bi}} \to n = 1|_{\text{mono}} \ldots$. We also see an effect of the effective potential barrier imposed by the A-type in the dispersive Landau levels near the interface. For a certain

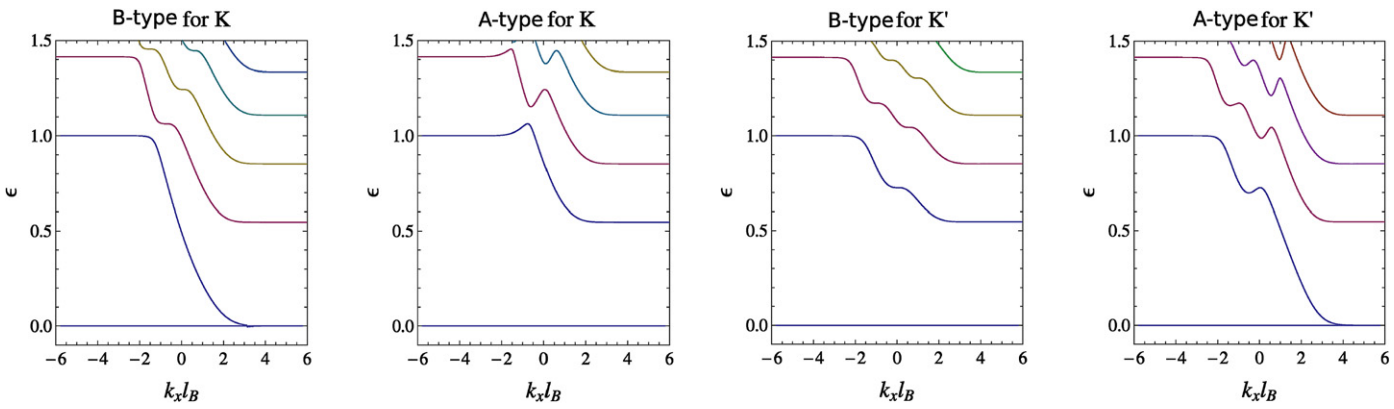

Fig. 4. (Color online.) The dispersion curve around Dirac cones in the presence of magnetic field. The upper two figures are for the B-type and A-type interfaces around one Dirac cone respectively, and the lower two figures are that for the other Dirac cone.

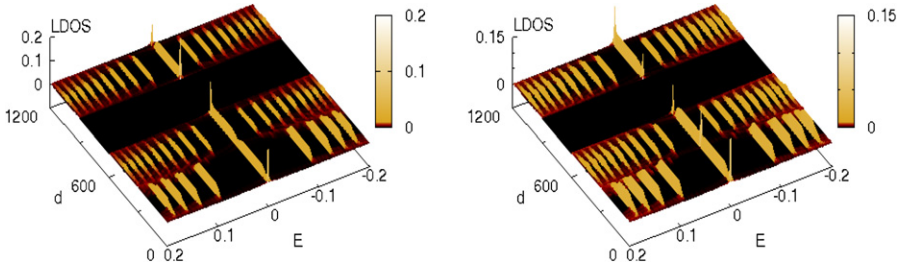

Fig. 5. The LDOS of the hybrid bilayer graphene with B-type (left) and A-type (right) edge in a magnetic field. The strength of the magnetic field is expressed as magnetic flux ϕ in each unit cell $\phi = \phi_0/1315$ (ϕ_0 is the magnetic flux quanta) which corresponds to $B \sim 60T$.

range of field strength the dispersion develops a local maximum for A-type while the B-type only develops a flat plateau feature.

Fig. 5 shows the LDOS for hybrid bilayer graphene in a magnetic field with B-type and A-type edge respectively from a numerical calculation of a system with width of 600 unit cells in y direction. The Landau level structures are clear in the bulk both in monolayer and bilayer graphene. Their mismatch induces dispersion along the interface. On the other hand, according to the analysis of the Dirac equation, it also shows the existence of the density peak at Fermi energy $E = 0$ only on the upper layer for B-type edge and on both two layers for A-type edge.

5. Discussion and conclusion

We study the edge state at the hybrid interface between monolayer and bilayer graphene both in zero field and in a magnetic field. There are two types of interface structures addressed by the B-type and A-type due to the type of the terminated atoms at the edge. We find the localized zero energy edge state always exists for both two types of interface whether in the presence of the magnetic field or not, however, the distribution of the edge state and the energy-momentum dispersion near the Dirac cone and the LDOS shows significantly different features to two types of hybrid edge. For B-type interface, the edge state only lives on the edge of the upper layer graphene which reflects as one LDOS peak at $E = 0$ in the upper layer. The edge state has weights on both two layers along the A-type interface. Thus, we observed the enhanced LDOS peak in the bottom layer also. The dispersion curve of the A-type edge develops strong anticrossing feature in the absence of magnetic field and local maximum in the presence of magnetic field which we explained as the effect of the effective potential imposed by dimer edge. Similar differences between B-type and A-type were also discussed in the calculation of transmission coefficients across the interface [31,33,34]. For the A-type edge the transmission probability is reduced significantly for incoming electrons with energy $E \sim t_\perp$ which can be interpreted in a similar way. We also show that in the presence of a magnetic field the dispersion of Landau levels continuously goes through the interface in different manners at two Dirac cones because of the inversion symmetry broken. Here we just consider the nearest interlayer interaction γ in Eq. (4) for simplicity. The other interlayer terms, such as the A_1–B_2 interaction $\gamma_3 \ll \gamma$ (which is at the upper right corners in Eq. (4)) are only relevant at weak fields. It has nontrivial effect in the bulk, such as the shift the energy of the Landau level and splitting of the Dirac point [35]. However, if we look at the zero energy solution of the Dirac equation, the differences of the relative weight of the wavefunction between two types of interfaces are still survives. For B-type, the amplitude of ϕ_{B1} is much smaller comparing to that of ϕ_{B2}, while for A-type edge, they are quite comparable. Therefore, the edge state properties are still dominated by γ, the dimer coupling.

In summary, the physical properties of hybrid graphene systems are mostly dominated by both that of the monolayer and bilayer graphene, and also how they are stacked. The existence of anticrossing in zero field and the dispersive Landau levels in the magnetic field near the interface could be related to the unexpected feature other than that of the monolayer or bilayer graphene in the magneto transport experiment [28]. Further study of the hybrid structures for a more realistic setup, like including edge disorder, gate voltage, etc., are needed to deeply understand the experimental data.

Acknowledgements

We wish to thank K. Yang and Y. Barlas for very helpful discussions. This work is supported by Fundamental Research Funds for the Central Universities CDJRC10300007 (Z.-X.H.) and NSF under Grant No. DMR-1004545 (W.X.D.).

References

[1] K.S. Novoselov, A.K. Geim, S.V. Morozov, D. Jiang, Y. Zhang, S.V. Dubonos, I.V. Grigorieva, A.A. Firsov, Science 306 (2004) 666.
[2] Y. Zhang, J.P. Small, W.V. Pontius, P. Kim, Appl. Phys. Lett. 86 (2005) 073104; Y. Zhang, J.P. Small, M.E.S. Amori, P. Kim, Phys. Rev. Lett. 94 (2005) 176803.
[3] J.S. Bunch, Y. Yaish, M. Brink, K. Bolotin, P.L. McEuen, Nano Lett. 5 (2005) 287.
[4] C. Berger, Z.M. Song, T.B. Li, X.B. Li, A.Y. Ogbazghi, R. Feng, Z.T. Dai, A.N. Marchenkov, E.H. Conrad, P.N. First, W.A. de Heer, J. Phys. Chem. B 108 (2004) 19912.
[5] K.S. Novoselov, D. Jiang, F. Schedin, T.J. Booth, V.V. Khotkevich, S.V. Morozov, A.K. Geim, Proc. Natl. Acad. Sci. USA 102 (2005) 10451.
[6] P.R. Wallace, Phys. Rev. 71 (1947) 622.
[7] K.S. Novoselov, A.K. Geim, S.V. Morozov, D. Jiang, M.I. Katsnelson, I.V. Grigorieva, S.V. Dubonos, A.A. Firsov, Nature 438 (2005) 197; K.S. Novoselov, E. McCann, S.V. Morozov, V.I. Falko, M.I. Katsnelson, U. Zeitler, D. Jiang, F. Schedin, A.K. Geim, Nature Physics 2 (2006) 177.
[8] Y. Zhang, Y.-W. Tan, H.L. Stormer, P. Kim, Nature 438 (2005) 201; Y. Zhang, Z. Jiang, J.P. Small, M.S. Purewal, Y.-W. Tan, M. Fazlollahi, J.D. Chudow, J.A. Jaszczak, H.L. Stormer, P. Kim, Phys. Rev. Lett. 96 (2006) 136806; Z. Jiang, Y. Zhang, H.L. Stormer, P. Kim, Phys. Rev. Lett. 99 (2007) 106802.
[9] K.S. Novoselov, Z. Jiang, Y. Zhang, S.V. Morozov, H.L. Stormer, U. Zeitler, J.C. Maan, G.S. Boebinger, P. Kim, A.K. Geim, Science 315 (2007) 1379.
[10] D.A. Abanin, K.S. Novoselov, U. Zeitler, P.A. Lee, A.K. Geim, L.S. Levitov, Phys. Rev. Lett. 98 (2007) 196806.
[11] A.H. Castro Neto, F. Guinea, N.M.R. Peres, K.S. Novoselov, A.K. Geim, Rev. Mod. Phys. 81 (2009) 109.
[12] S.E. Stein, R.L. Brown, J. Am. Chem. Soc. 109 (1987) 3721.
[13] K. Tanaka, S. Yamashita, H. Yamabe, T. Yamabe, Synth. Met. 17 (1987) 143.
[14] M. Fujita, M. Yoshida, K. Nakada, Fullerene Sci. Technol. 4 (1996) 565.
[15] M. Fujita, K. Wakabayashi, K. Nakada, K. Kusakabe, J. Phys. Soc. Jpn. 65 (1996) 1920.
[16] K. Nakada, M. Fujita, G. Dresselhaus, M.S. Dresselhaus, Phys. Rev. B 54 (1996) 17954.
[17] H.-X. Zheng, Z.F. Wang, T. Luo, Q.W. Shi, J. Chen, Phys. Rev. B 75 (2007) 165414.
[18] L. Brey, H.A. Fertig, Phys. Rev. B 73 (2006) 195408; Phys. Rev. B 73 (2006) 235411; H.A. Fertig, L. Brey, Phys. Rev. Lett. 97 (2006) 116805.
[19] N.M.R. Peres, F. Guinea, A.H. Castro Neto, Phys. Rev. B 73 (2006) 125411.
[20] M. Kohmoto, Y. Hasegawa, Phys. Rev. B 76 (2007) 205402.
[21] S. Ryu, Y. Hatsugai, Phys. Rev. Lett. 89 (2002) 077002.
[22] K. Sasaki, S. Murakami, R. Saito, Appl. Phys. Lett. 88 (2006) 113110.
[23] K. Sasaki, K. Sato, R. Saito, J. Jiang, S. Onari, Y. Tanaka, Phys. Rev. B 75 (2007) 235430.
[24] A.H. Castro Neto, F. Guinea, N.M.R. Peres, Phys. Rev. B 73 (2006) 205408.
[25] Y. Niimi, T. Matsui, H. Kambara, K. Tagami, M. Tsukada, H. Fukuyama, Phys. Rev. B 73 (2006) 085421.
[26] Y. Kobayashi, K.I. Fukui, T. Enoki, K. Kusakabe, Y. Kaburagi, Phys. Rev. B 71 (2005) 193406.
[27] H.P. Dahal, Z.-X. Hu, N.A. Sinitsyn, K. Yang, A.V. Balatsky, Phys. Rev. B 81 (2010) 155406.
[28] C.P. Puls, N.E. Staley, Y. Liu, Phys. Rev. B 79 (2009) 235415.
[29] The abstract is available online at http://meetings.aps.org/Meeting/MAR10/Event/119769.
[30] E.V. Castro, N.M.R. Peres, J.M.B.L. Santos, Europhys. Lett. 84 (2008) 17001.
[31] J. Nilsson, A.H. Castro Neto, F. Guinea, N.M.R. Peres, Phys. Rev. B 76 (2007) 165416.
[32] M. Koshino, T. Nakanishi, T. Ando, Phys. Rev. B 82 (2010) 205436.
[33] T. Nakanishi, M. Koshino, T. Ando, Phys. Rev. B 82 (2010) 125428.
[34] W.X. Ding, unpublished.
[35] A.H. Castro Neto, F. Guinea, N.M.R. Peres, K.S. Novoselov, A.K. Geim, Rev. Mod. Phys. 81 (2009) 109.